ORIGINAL PAPER

Journal of Anatomy · ANATOMICAL SOCIETY WILEY

Dimensional study of prostate cancer using stereological tools

Luis Santamaría[1] | Ildefonso Ingelmo[2] | Fernando Teba[3]

[1]Department of Anatomy, Histology, and Neuroscience, School of Medicine, Autonomous University of Madrid, Madrid, Spain

[2]Department of Anesthesiology, Hospital Ramón y Cajal, Madrid, Spain

[3]Department of Surgery (Urology), Hospital de La Princesa, School of Medicine, Autonomous University of Madrid, Madrid, Spain

Correspondence
Luis Santamaría, Department of Anatomy, Histology, and Neuroscience, School of Medicine, Autonomous University of Madrid, C/Arzobispo Morcillo 2, 28029 Madrid, Spain.
Email: luis.santamaria@uam.es

Abstract

This study analyzes the dimensional changes of the glands from prostate cancer by applying stereology to estimate the variations in volume, length, surface, and cellular densities of tumor acini. Normal and tumor acini were visualized using immunohistochemistry for cytokeratin18. On immunostained sections, parameters related to the dimensions and cell population of prostate acini were measured. The immunohistochemical expression of proliferative cell nuclear antigen was also measured to correlate the quantitative changes estimated with the proliferative activity of the epithelium. The average cell volume in normal and tumor epithelium was estimated using the method of the nucleator. The relative size of the acini was similar in the carcinoma compared with the normal prostate. Within the acini, the fraction of acinar volume occupied by the epithelium was significantly higher in cancer than in the nontumor prostate. Conversely, the glandular lumen of the cancer acini is lower than in the normal acini. The significant increase of acinar length density in the carcinoma indicates that the glandular tree's growth in the carcinoma is higher and with more branches than in the case of nonneoplastic glands. The basal surface density is higher in the carcinoma than in the controls. The number of epithelial cells per unit length of acini was significantly decreased in the neoplastic glands. This "dilution" of the cell population along the cancer acinus can be explained by the significant increase in the tumor cell's mean cell volume.

KEYWORDS
acinar length density, prostate cancer, relative volumes, stereology, surface densities

1 | INTRODUCTION

Prostate cancer remains a common carcinoma affecting the male population (Coloma et al., 2014). Little is known about the nature and variability of dimensional changes in the structure of tumor glands and their relationship with cancer behavior. All factors related (Humphrey, 2004; Iczkowski, et al., 2011; Tolkach & Kristiansen, 2018) to the development of prostate cancer configure the tumor's phenotype, with features that can be quantified by stereology (Mattfeldt et al., 2004; Santamaria et al., 2017, 2018).

Three-dimensional reconstruction techniques, supported by confocal microscopy, have been used to investigate the spatial characteristics of the growth of prostate lesions (van Royen et al., 2016), rendering data about the 3D features of cancer growth. The 3D analysis of prostate cancer is interesting because it has contributed to establishing various architectural subgroups (Verhoef et al., 2019). The approach mentioned above provides interesting information about the three-dimensional structure of the normal and pathological acinar tree; however, these studies do not provide quantitative data on other elements of the acini geometry such as

the volumes, lengths, and surfaces of the acinar structure, in relation to a reference space (i.e. prostate volume). This information can only be obtained reliably through stereological methods (Baddeley and Vedel Jensen 2005a, 2005b, 2005c).

Therefore, the main objective of this study consists in the analysis of the dimensional changes of the glands from prostate cancer through the unbiased application of stereological tools to estimate the variations in volume densities of tumor acini, changes in the glands' lengths, and surface density at the luminal and basal level of the acini.

These tools have been widely applied in morphological studies in normal and pathological human prostate (Mattfeldt et al., 2003; Santamaria et al., 2016; Santamaria Solis et al., 2015) and laboratory animals in prostate development (Buzzell, 1985; Vilamaior et al., 2006), and experimental conditions (Aminsharifi et al., 2016; Eslahi et al., 2017; Ribeiro et al., 2008).

Several stereological parameters related to prostatic acini's size and conformation were evaluated in both normal human and pathological (carcinoma) prostates to meet the objectives referred to above.

Several studies using monoclonal anti-cytokeratin antibodies in prostate have differentiated the columnar and basal cell populations by their specific cytokeratin content (Brawer et al., 1985; Schlegel et al., 1980). The columnar cells react with monoclonal antibodies to cytokeratin 18 (ck18) (Nagle et al., 1987). Besides, chemical determination of the cytokeratin phenotype of three established human prostatic carcinoma cell lines also suggests that all three cell lines synthesize ck18 (Nagle et al., 1987). Therefore, normal and tumor acini were visualized using immunohistochemistry for ck18 (Santamaria Solis et al., 2015). On ck18 immunostained sections, several parameters related to the dimensions and cell population of normal and neoplastic prostatic acini were measured. The immunohistochemical expression of PCNA (proliferative cell nuclear antigen) was measured using the labeling index (LiPCNA) (Gomez et al., 2009) to correlate the quantitative changes estimated with the epithelium's proliferative activity. The average cell volume ($V_N$cell) in normal and tumor epithelium was also calculated using the stereological method of the nucleator (Howard & Reed, 2005). All parameters were summarized in Table 1. Furthermore, an explanation of each of the stereological parameters used in practical terms is provided in Table 2.

TABLE 1 Stereological parameters employed

Volume fractions[a]	Densities of length and acinar surface[b]	Numerical densities[c]	Others[d]
$V_V$acini	$L_V$acini	$N_V$ep	LiPCNA
$V_V$lumen	$S_V$lumen	$N_L$ep	$V_N$cell
$V_V$ep	$S_V$basal		

[a]Volume fractions of acini ($V_V$acini), lumen ($V_V$lumen), and epithelium ($V_V$ep).
[b]Acinar length per unit of prostate volume ($L_V$acini), lumen surface per unit of prostate volume ($S_V$lumen), and basal acinar surface per unit of prostate volume ($S_V$basal).
[c]Epithelial cell number per unit of prostate volume ($N_V$ep), and epithelial cell number per acinar length unit ($N_L$ep).
[d]PCNA labeling index of epithelial cells (LiPCNA) and average cell volume of epithelial cells ($V_N$cell).

2 | METHODS

2.1 | Material

Twenty prostate specimens were collected from La Princesa Hospital, 10 were from adults, (CTR), age (mean ± SD): 45 ± 7; range: 30–47 years, all these specimens were of healthy subjects, without endocrine or reproductive pathology, deceased in traffic accidents, and eligible as donors for transplant. The other 10 were surgical specimens (radical prostatectomy) from patients diagnosed with prostate carcinoma (CA): age (mean ± SD): 70 ± 10, range: 56–85 years. The diagnosis was confirmed by histopathology. Cancer cases were graded according to Gleason score (Egevad et al., 2012; Epstein et al., 2005); only cases with a grade of 7(3 + 4) or 7(4 + 3) were included in the study. All cases were without prior neoadjuvant hormonal therapy. Ethical requirements informed consent issued by the Bioethics Committee of the Hospital Universitario de La Princesa (Madrid, Spain)-were accomplished to obtain the prostate tissue either when the multi-organic extraction for transplant (CTR) or at the surgery (CA).

2.2 | Processing of the tissues

The specimens were fixed for a week in 10% paraformaldehyde in PBS, pH 7.4. After fixation, each specimen from the two groups was segmented into two halves. One of the fragments was thoroughly sectioned into 2-mm-thick slices, performed by isotropic uniform random sampling (IUR sections) (Howard & Reed, 2005) to preserve the isotropy of the tissue to implement all stereological estimates except for surface density measurements. Vertical uniform random sections (VUR) were obtained on the other half of each specimen (of the same thickness as the IUR sections; Baddeley and Vedel Jensen 2005a, 2005b, 2005c) to estimate surface density measurements. All the slices (IUR and VUR) were processed for paraffin embedding. Thirty sections (5-μm-thick) were performed on each block for immunohistochemistry. Fifteen additional thicker sections (10-μm-thick) were obtained on each block from IUR sampling to estimate the numerical density of the epithelial cells.

2.3 | Immunohistochemistry

At least 20 randomly selected slides (10 IUR and 10 VUR samples) per specimen were immunostained in CTR and CA groups to detect ck18 and PCNA immunoreactivities. Sections were incubated with a monoclonal anti-cytokeratin 18 antibody (Abcam) diluted at 1:250 and with a monoclonal anti-PCNA antibody (Biomeda) diluted at 1:200. Pretreatment of sections by heat (Martin et al., 2001) was performed to enhance ck18 immunostaining. After incubation with the specific biotinylated secondary antibodies, the sections were treated with a streptavidin-biotin-peroxidase complex (Biomeda). The immunostaining reaction product was then developed using

TABLE 2 Explanation about the stereological parameters employed.

Volume fractions	Definition	Densities of length and acinar surface	Definition	Numerical densities	Definition	Others	Definition
$V_V$acini, $V_V$lumen, $V_V$ep	Volume proportion of one phase (acini, lumen, epithelium) within a reference volume (prostate volume)	$L_V$acini, $S_V$lumen, $S_V$basal	Length of a linear element (acinar structure) or the area of an interface (luminal or basal) within a reference volume unit (prostate volume)	$N_V$ep, $N_L$ep	Number of discrete objects (epithelial cells) in a unit of the reference space, either acinar volume (N_V) or acinar structure length (N_L)	LiPCNA, $V_N$cell	PCNA labeling index is the ratio between the number of immunoreactive PCNA nuclei and the total number of nuclei in a cell population. The average cell volume ($V_N$cell) is the mean size of particles (cells) sampled from a population

Note: The conceptual definitions of parameters (Volume fractions, Densities of length and acinar surface, Numerical densities, Labeling index of PCNA, and average cell volume of epithelial cells), are specified.

diaminobenzidine (DAB) (Sigma). Rationals for immunohistochemistry have been widely described in other studies, either for PCNA (Gomez et al., 2009; Santamaria et al., 2009, 2017), or for ck18 immunostaining (Santamaria et al., 2018).

2.4 | Quantitative methods

For calculation of dimensional parameters indicated in Table 1, the rationale was as follows: ck18 immunostained images were captured at a final magnification of X240, from an average of 20 systematically randomly sampled light microscopic fields in five systematically randomly selected sections of each sampling protocol (IUR and VUR) in each specimen from each group. The images were captured using a color digital camera, DP 70 (Olympus Corporation of the Americas) with a resolution of 12.5 megapixels, attached to an Olympus microscope fitted with a motorized stage controlled by the stereological software Cast-Grid (Stereology Software Package). This program monitors the XY displacement of the microscope stage and allows the selection of fields to be studied by systematic random sampling after selecting an appropriate sampling fraction (Santamaria Solis et al., 2015).

The volume fractions, that is, the ratio between interest area and the reference area, were measured in all the captured images from the IUR sections immunostained to ck18 according to the following procedure. To estimate the areas (total, acinar, and lumen), the STEPanizer program was employed, which is a software for the stereological assessment of digitally captured images (Tschanz et al., 2011). This software superimposes a regularly spaced point frame on the images, whose point associated area a(p) was settled to 10,414 μm^2. The number of points hitting in the different tissue compartments was recorded and used for the calculation of the volume fractions as indicated below:

$$V_V acini = \frac{\sum P(\text{acinar points})}{\sum P(\text{total points: acini} + \text{stromal tissue})}$$

$$V_V lumen = \frac{\sum P(\text{lumen points})}{\sum P(\text{acinar points})}$$

$$V_V ep = 1 - V_V lumen$$

The linear and surface densities, that is, the length of the acinar structure per unit of volume, and the luminal and basal surface of the acini per unit of volume were estimated in all the captured images either from IUR ($L_V$acini) or VUR ($S_V$lumen, $S_V$basal) sections immunostained to ck18 using the STEPanizer software and following the subsequent procedures. In the case of $L_V$acini, the total tissue (stromal + acinar compartments) was considered as reference space. The acinar profiles immunostained to ck18 eligible for counting were sampled by a disector frame and fulfilling the Sterio rule (Sterio, 1984; Figure 1a). The $L_V$acini was calculated by the formula:

$$L_V acini = \frac{2 \times \sum Q^-}{\sum A}$$
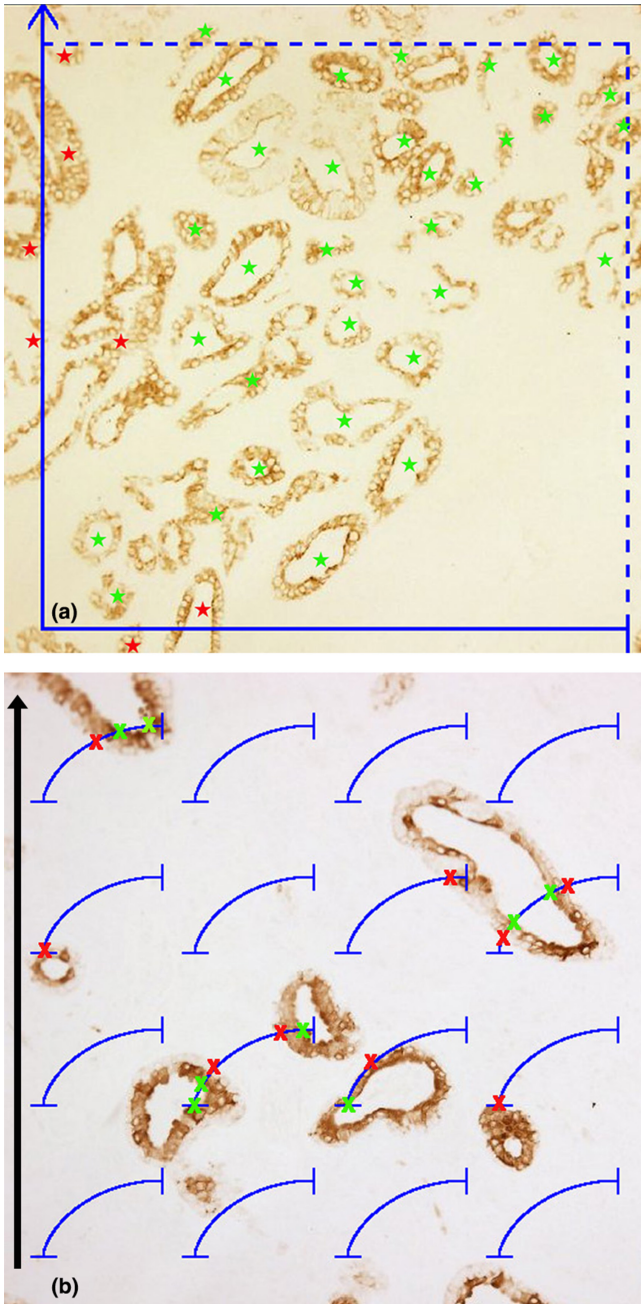
(a)

(b)

FIGURE 1 (a) Shows an example of the estimate of the density of length ($L_V$acini) on an image of prostate cancer immunostained for ck18. An unbiased counting frame is superimposed (blue): the solid lines are the sides of exclusion, and those with dotted lines, those of inclusion, according to Sterio's rule. The immunostained profiles marked with green stars are included in the count, and those marked with red stars are excluded. (b) Shows an example of the estimation of surface densities ($S_V$basal, $S_V$lumen) on an image of prostate cancer immunostained for ck18. Onto the picture is superimposed (blue) a frame constituted by cycloids with its minor axis parallel to the vertical axis of the section (black arrow in the left margin of the image). The green marks show the intersection of the cycloids with the luminal zone of the profile (I lumen); the red marks indicate the cycloid intersection with the basal zone (I basal)

where Q^- = number of eligible acinar profiles and $\sum A$ = total sampled, that is, area of disector frame (325,676 µm^2) multiplied by the number of selected frames.

In the case of S_V, two parameters were evaluated: the luminal area per unit of prostatic volume ($S_V$lumen) and the basal area of the acini per unit of prostate volume ($S_V$basal). The reference space chosen was the same as for $L_V$acini. The software (Figure 1b) superimposes on the VUR ck18 immunostained sections a cycloid frame (West, 2012) whose length associated point was settled to $l(p)$ =76 µm. The S_V (either luminal or basal) was calculated by the formula:

$$S_V = \frac{2 \times \sum I}{\sum P \times l(p)}$$

where I is the number of intersections of cycloid curves with the acinar profiles (lumen contours to $S_V$lumen, and basal contours of the acinus to $S_V$basal); P = number of points that mark the ends of the cycloid curve and that fall on the reference space, the area associated with those points was $a(p)$ = 11,487 µm^2, and $l(p)$ =76 µm. Each VUR section measured was oriented so that its vertical axis was parallel to the minor axis of the frame's cycloid curves (Figure 1b; Baddeley and Vedel Jensen 2005a, 2005b, 2005c; Howard & Reed, 2005).

Estimates of the relative number of epithelial cells and cells PCNA immunoreactive were calculated onto IUR 10-µm-thick sections, using the optical disector (Gundersen et al., 1988; Howard & Reed, 2005). Measurements were carried out using an Olympus microscope fitted with a motorized stage and equipped with an ×100 oil immersion lens (numerical aperture of 1.4) at a final magnification of ×1200, employing the stereological software Cast-Grid. An average of 100 fields per section was scanned in each group. The software superimposes a disector frame onto the images captured by the video camera. A microcator measured the Z displacement of the samples (Haidenhain, Transreut, Germany) adapted to the stage's vertical axis.

In each selected field, the acinar epithelium area was scanned, and the numerical densities of both total ($N_V$ep) and PCNA+ ($N_V$epPCNA) epithelial cells were evaluated, counting their nuclei, according to the Sterio rule (Sterio, 1984).

The N_V is determined by the formula:

$$N_V ep = \frac{\sum Q^-}{\sum V dis}$$

where: Q^- = number of eligible nuclei, Vdis = volume of disectors in which the upper-right corner hits epithelial tissue.

The labeling index for PCNA (LiPCNA) was then calculated:

$$LiPCNA = \frac{N_V PCNA}{N_V ep}$$

After estimation of $N_V$ep, the epithelial cell number per unit of acinar length ($N_L$ep) was calculated according to the formula:

$$N_L ep = \frac{N_V ep}{L_V \text{acini}}$$

The nucleator (Sorensen, 1991) was applied on the 10-μm-thick IUR sections to estimate the $V_N$cell in the prostate epithelium from both study groups. Briefly, the epithelial nuclei were the sampling unit to measure $V_N$cell. The nuclei eligible for estimate the cell volume were sampled after the Sterio rule using optical disectors at a final magnification of ×1200. A random point located inside each nucleus was selected as the reference point. Through this point, the software generates two isotropically oriented segments hitting four points from the cytoplasm boundary. The program then employs the following formula to estimate the volume:

$$V_N \text{cell} = \frac{4\pi}{3} \times l^3_n$$

$V_N$cell is the average cell volume, and l^3_n is the mean cubed length of the segments intercepting the cytoplasm boundary. These measurements also employed the same microscopic system controlled by the stereological software Cast-Grid already used to estimate the epithelial cells' numerical densities.

2.5 | Statistical methods

The parameters measured were expressed as mean ± SEM. Comparisons between the means from CTR and CA groups were performed by a Student t-test ($p < 0.05$). The results were represented graphically by scatter plots, using Prism 7.00 (Graph-Pad Software).

3 | RESULTS

In both the CTR and CA cases, the immunostaining for ck18 was expressed exclusively in the prostatic epithelium in columnar and basal cells. Neither the intensity nor the immunostaining location showed qualitative differences between both groups (Figure 2a,b). In CTR, few immunoreactive nuclei were detected for PCNA, located at the basal cell layer level (Figure 2c). In CA, abundant nuclei immunostained for PCNA were observed in the tumor acini (Figure 2d). No significant differences were observed between CTR and CA when comparing the $V_V$acini (Figure 3a). The $V_V$ep was significantly higher in CA than in CTR (Figure 3b).

Conversely, $V_V$lumen was significantly higher in CTR than in CA (Figure 3c). $L_V$acini of CA was significantly greater than in CTR (Figure 4a). $S_V$lumen did not show significant differences between
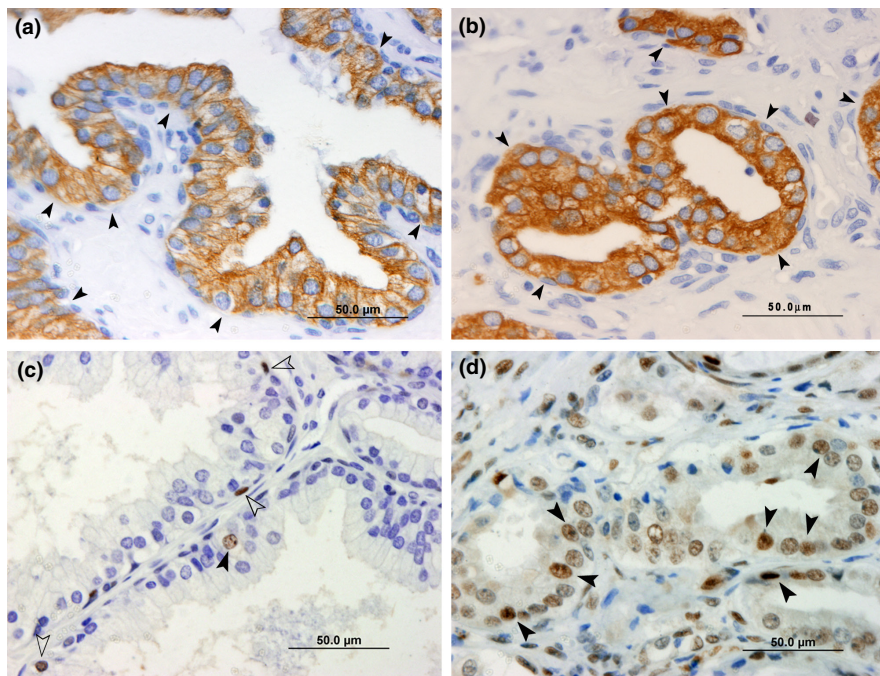

FIGURE 2 (a, b) Images of a specimen of the CTR group (a) and another of CA (b) immunostained for cytokeratin 18 (ck18). In both normal prostate and cancer, immunoreactivity for ck18 was observed exclusively in the epithelium of acini (solid arrowheads). No qualitative differences between both groups were observed. Immunostaining to PCNA was shown in (c) for CTR group and (d) for CA group. Immunoreactive nuclei were detected in CTR, located at the basal cell layer level (empty arrowheads). Occasional nuclei of columnar cells also show immunostaining for PCNA (solid arrowhead), while in CA, abundant nuclei immunostained for PCNA were observed in the tumor acini (solid arrowheads). In all the images, the calibration bars represent 50 μm [Colour figure can be viewed at wileyonlinelibrary.com]

CTR and CA (Figure 4b). However, $S_V$basal was significantly higher in CA than in CTR (Figure 4c).

N_V ep did not show significant differences between CTR and CA (Figure 5a). However, $N_L$ep was significantly lower in CA than CTR (Figure 5b). Furthermore, LiPCNA showed a significant increase in CA compared with the CTR (Figure 6). Regarding $V_N$cell, a significant increase in CA was found when compared with CTR (Figure 7).

Table 3 presents a brief summary of the differences and similarities between normal and cancerous tissue in terms of stereological parameters.

4 | DISCUSSION

Some authors have described an increase in the partial epithelial volume in cancer compared with that observed in nontumor prostate (Bourne et al., 2012); this appears in contrast to the present study's findings, which does not show significant differences between the $V_V$ep in cancer and controls. In the work of Bourne et al. (2012) a magnetic resonance microimaging system was employed to estimate

the volumes (Bourne et al., 2012). Besides, the equivalence between what these authors call "partial volumes of the analyzed compartments" and the $V_V$acini estimated by stereology in our study is not clear. Furthermore, the study mentioned above does not define the reference space for the determination of partial volumes.

The growth of the glandular tree (per unit volume) in the carcinoma is higher and with more branches than in nonneoplastic glands; this is indicated by the significant increase of $L_V$acini in the carcinoma. As it has been seen that $V_V$acini is similar in cancer and controls, the rise of $L_V$acini in cancer entails a greater folding of the tumor glandular tubes so that they occupy a relative volume similar to that of the nontumor glands.

$S_V$basal is higher in the carcinoma than in the controls. This phenomenon may result from the increase in acinar length density and involves a greater surface of exchange between cancer acinus and stromal vessels. Perhaps the rise in the blood PSA detected in prostate cancer can be partially explained by this factor. This increment of $S_V$basal and increased permeability of the basement membrane also seems important when related to the microvessel density described in prostate cancer (Barth et al., 1997; Coloma et al., 2014;
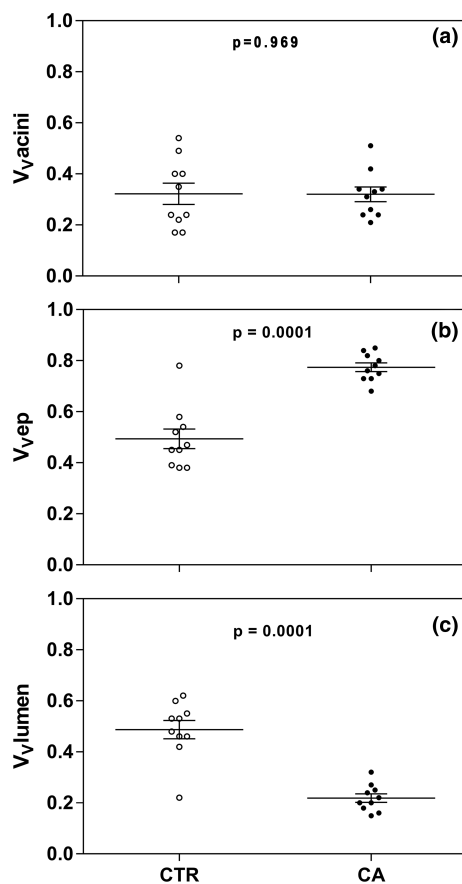

FIGURE 3 Scatter plots to mean ± SD of volume fractions in normal prostate (CTR) and carcinoma (CA) for (a) total acini ($V_V$acini); (b) epithelium ($V_V$ep); (c) acinar lumen ($V_V$lumen). In (a) the differences between CTR and CA are not significant ($p = 0.969$). In (b) and (c), the differences between CTR and CA are significant ($p = 0.0001$). The individual values are represented in CTR by empty circles and in CA by solid circles
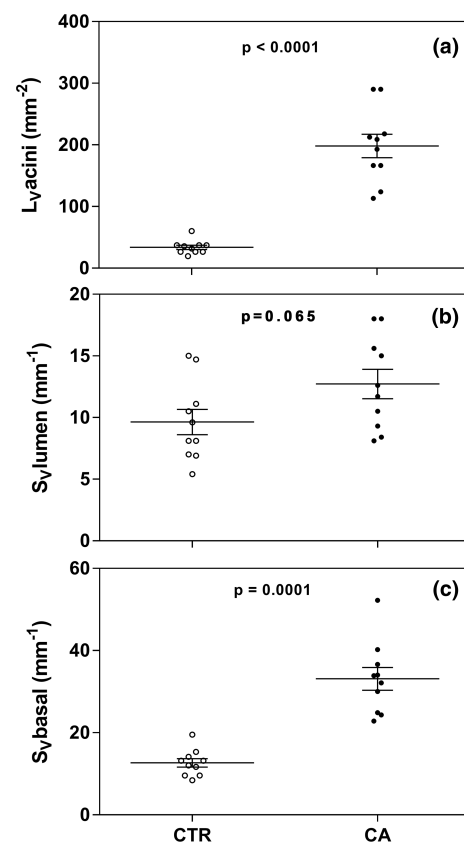

FIGURE 4 Scatter plots to mean ± SD, for (a) acinar length density ($L_V$acini); (b) luminal surface density ($S_V$lumen); (c) basal surface density ($S_V$basal) in normal prostate (CTR) and carcinoma (CA). In (a), the differences between CTR and CA are significant ($p < 0.0001$). In (b), the differences between CTR and CA are not significant ($p = 0.065$). In (c), the differences between CTR and CA are significant ($p = 0.0001$). The individual values are represented in CTR by empty circles and in CA by solid circles

Santamaria et al., 2011). It may be a factor that intervenes in the spread of the tumor. However, the $S_V$lumen of the cancer acini is similar to that observed in normal acini, and this is consistent with the scarcity of light detected in neoplastic acini (Verhoef et al., 2019).

How do the revealed structural changes correlate with the dynamics of the neoplastic cell population? PCNA has long been known to be a good marker of cell proliferation in prostate cancer (Botticelli et al., 1993, 1998). It has been observed in this study that the increment in cell proliferation shown by the significant increase
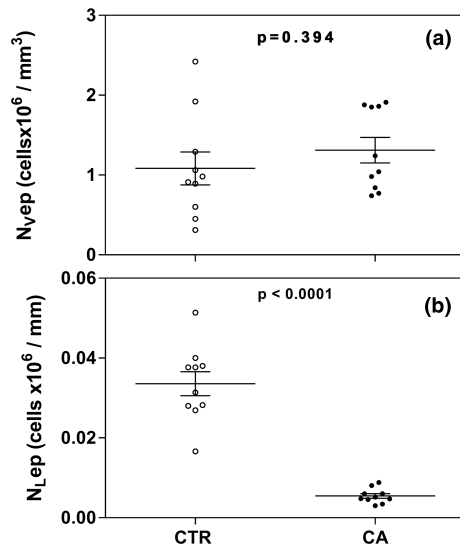

FIGURE 7 Scatter plot to mean ± SD, average cell volume of epithelial cells ($V_N$cell) in normal prostate (CTR) and carcinoma (CA). The differences between CTR and CA are significant ($p = 0.03$). The individual values are represented in CTR by empty circles and in CA by solid circles

FIGURE 5 Scatter plots to mean ± SD, for (a) number of epithelial cells for the unit of volume ($N_V$ep); (b) the number of epithelial cells for the unit of acinar length ($N_L$ep), in normal prostate (CTR) and carcinoma (CA). In (a), the differences between CTR and CA are not significant ($p = 0.394$). In (b), the differences between CTR and CA are significant ($p < 0.0001$). The individual values are represented in CTR by empty circles and in CA by solid circles
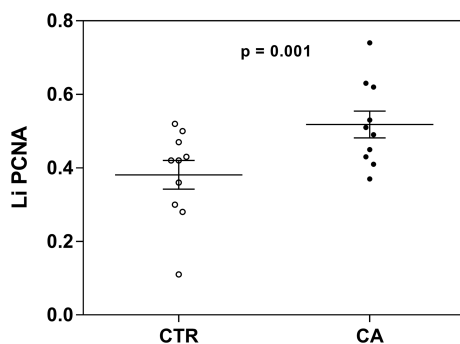

FIGURE 6 Scatter plot to mean ± SD, for labeling index of PCNA of the epithelium (LiPCNA), in normal prostate (CTR) and carcinoma (CA). The differences between CTR and CA are significant ($p = 0.001$). The individual values are represented in CTR by empty circles and in CA by solid circles
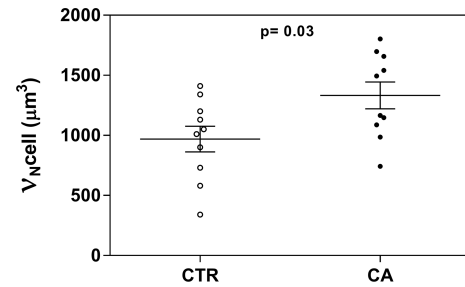
in LiPCNA in cancer does not result in a significant increment in the $N_V$ep compared with normal epithelium.

It is known that the balance between apoptosis and proliferation is under the influence of numerous agents (Fontana et al., 2019). A possible explanation for the fact that the relative number of epithelial cells was similar in controls and cancer can be related to increased tumor apoptosis, which balances the cell population's rising; however, most of the studies on apoptosis in prostate cancer suggests that tumor cells show a decrease in the rate of programed cell death (Mohammad et al., 2015; Winter et al., 2001). Another possible explanation for the findings indicated above is related to dimensional changes: The volume occupied by tumor epithelium is greater than that of normal epithelium when both are estimated taking acinar volume as a reference; then, the numerical density of epithelial cells remains similar in CA and CTR, although the number of epithelial cells increases in cancer, the volume of the tumor epithelium also increases compared with the normal epithelium, so the ratio between cell number and acinar volume would remain similar in CTR and CA. Everything mentioned above emphasizes the importance of considering the reference volume when the size of the cell population is estimated (Baddeley and Vedel Jensen, 2005a, 2005b, 2005c).

The use of stereological tools such as the nucleator (Howard & Reed, 2005) for the estimation of cell volumes has been carried out in various animal models or human pathology in different organs or tissues, particularly in the field of neuroscience (Chen et al., 2020; Panahi et al., 2017; Real et al., 2020). There are studies on estimating the volume-weighted nuclear volume in prostatic tumor pathology and related to the prognosis and cancer grading (Leze et al., 2014). However, no studies have been found that analyze the changes in the volume occupied by the cytoplasm of cancer cells versus normal epithelial cells using stereology. Although there are recent studies on the variability of tumor cell sizes applying single-cell analysis methodology on liquid biopsies (Lambros et al., 2018; Park et al., 2014; Wang et al., 2000), their findings cannot be extrapolated to what was observed applying conventional histology.

A significant increase in $V_N$cell was detected in our study in cancer compared with the controls. This increase in cell size in the tumor may

TABLE 3 Summary of quantitative differences between normal and cancer tissue

Parameter	Quantitative morphological differences
Volume proportion of acini within the prostate volume ($V_V$acini)	No differences between normal and carcinoma tissue
Volume proportion of epithelium within the acinar volume ($V_V$ep)	Greater in carcinoma than in normal tissue
Volume proportion of lumen within the acinar volume ($V_V$lumen)	Greater in normal tissue than in carcinoma
Length of an acinar structure per unit of prostate volume ($L_V$acini)	Greater in carcinoma than in normal tissue
Area of lumen interface per unit of acinar volume ($S_V$lumen)	No differences between normal and carcinoma tissue
Area of basal interface per unit of acinar volume ($S_V$basal)	Greater in carcinoma than in normal tissue
Number of epithelial cells per unit of acinar volume ($N_V$ep)	No differences between normal and carcinoma tissue
Number of epithelial cells per unit of length of the acinar structure ($N_L$ep)	Less in carcinoma than in normal tissue
The ratio between the number of immunoreactive PCNA nuclei and the total number of epithelial nuclei (LiPCNA)	Greater in carcinoma than in normal tissue
Mean size of cells sampled from an epithelial population ($V_N$cell)	Greater in carcinoma than in normal tissue

Note: The quantitative differences between normal tissue (CTR group) and cancer (CA group) that appear in the right column are always significant ($p < 0.05$).

be the origin of the increase in the volume fraction of the acini occupied by the epithelium, already mentioned. Interestingly, the $N_L$ep was significantly decreased in the neoplastic glands. This "dilution" of the cell population along the cancer acinus can be explained by the significant increase in the $V_N$cell of the tumor cell since an increase in their size would cause them to be more spaced along the glandular tube.

From all of the above, it can be concluded that the dimensional changes described in cancers with Gleason pattern 7 can be compared with the three-dimensional characteristics of prostate cancer described by other studies (Verhoef et al., 2019). The increase in glandular length density and the decrease $V_V$lumen observed correlate well with the patterns of a continuum of interconnecting tubules (Verhoef et al., 2019).

In summary, two findings of this study can be put in relation to a greater aggressiveness of prostate cancer:

1. The increase in the relative length of the acinar tree (indicative of active growth of the glandular component) that results in the folding of the acinar structure within a small reference volume originating a pattern of small, closely packed, uniform glands in essentially circumscribed masses, frequently described in cancers with different Gleason grades (Egevad et al., 2012).
2. The increase in the relative basal surface of the neoplastic acini may be a factor intervening in the spread of the tumor. It could be related to the mode of infiltration of prostate carcinoma that is rather unique, as neoplastic glands mingle with benign glands, rendering the invasion front of this tumor intricate and irregular in comparison with other solid tumors that show a more circumscribed invasion front (Tolkach & Kristiansen, 2018).

AUTHOR CONTRIBUTIONS

All the authors have directly participated in the planning, execution, and analysis of the present paper, as indicated below: Luis Santamaría was involved in planning and study design, direction of stereological work, elaboration and analysis of discussion, and conclusions. Ildefonso Ingelmo was involved in search for bibliography, the capture, and process of the images. Fernando Teba was involved in study and collection of the cases from La Princesa Hospital and histological processing of the specimens.

DATA AVAILABILITY STATEMENT

The data that supports the findings of this study are available in this article as tables and figures.

ORCID

Luis Santamaría https://orcid.org/0000-0001-6560-2502

REFERENCES

Aminsharifi, A., Salehi, A., Noorafshan, A., Aminsharifi, A. & Alnajar, K. (2016) Effect of preoperative finasteride on the volume or length density of prostate vessels, intraoperative, postoperative blood loss during and after monopolar transurethral resection of prostate: a dose escalation randomized clinical trial using stereolog methods. *Urology Journal*, 13(1), 2562–2568. https://doi.org/10.22037/uj.v13i1.3107

Baddeley, A. & Vedel Jensen, E.B. (Eds.) (2005a). Introduction: plan of the book. In: *Stereology for statisticians*. Boca Ratón, FL: Chapman & Hall/CRC. pp. 1.

Baddeley, A. & Vedel Jensen, E.B. Eds. (2005b). Overview of modern stereology. In: *Stereology for statisticians*. Boca Ratón, FL: Chapman & Hall/CRC, pp. 55–85.

Baddeley, A. & Vedel Jensen, E.B. (2005c) *Stereology for statisticians*. Boca Ratón, FL: Chapman & Hall/CRC, pp. 1–395.

Barth, P.J., Ghafouri-Sanati, H., Kohler, H.H., Bittinger, A. & Riedmiller, H. (1997) Histological determinants of the vascular surface in prostatic carcinoma. *Urological Research*, 25(5), 303–308. https://doi.org/10.1007/BF01294655.

Botticelli, A.R., Casali, A.M., Botticelli, L. & Zaffe, D. (1998) Immunohistochemical detection of cell-cycle associated markers on paraffin embedded and formalin fixed needle biopsies

of prostate cancer: correlation of p120 protein expression with AgNOR, PCNA/cyclin, Ki-67/MIB1 proliferation-scores and Gleason gradings. *European Journal of Histochemistry*, 42(1), 41–48.

Botticelli, A.R., Criscuolo, M., Martinelli, A.M., Botticelli, L., Filoni, A. & Migaldi, M. (1993) Proliferating cell nuclear antigen/cyclin in incidental carcinoma of the prostate. *Virchows Archiv A, Pathological Anatomy and Histopathology*, 423(5), 365–368. https://doi.org/10.1007/BF01607149.

Bourne, R.M., Kurniawan, N., Cowin, G., Stait-Gardner, T., Sved, P., Watson, G. et al. (2012) Microscopic diffusivity compartmentation in formalin-fixed prostate tissue. *Magnetic Resonance in Medicine*, 68(2), 614–620. https://doi.org/10.1002/mrm.23244

Brawer, M.K., Peehl, D.M., Stamey, T.A. & Bostwick, D.G. (1985) Keratin immunoreactivity in the benign and neoplastic human prostate. *Cancer Research*, 45(8), 3663–3667.

Buzzell, G.R. (1985) Light-microscopic stereology for the study of the ventral and dorsal prostates of the Syrian hamster: strategy, techniques, and applications. *American Journal of Anatomy*, 173(4), 299–308. https://doi.org/10.1002/aja.1001730406.

Chen, F., Bertelsen, A.B., Holm, I.E., Nyengaard, J.R., Rosenberg, R. & Dorph-Petersen, K.A. (2020) Hippocampal volume and cell number in depression, schizophrenia, and suicide subjects. *Brain Research*, 1727, 146546. https://doi.org/10.1016/j.brainres.2019.146546.

Coloma, A., Codesal, J., Ingelmo, I., Ruiz, J., Teba, F., Pozuelo, J.M. et al. (2014) Stereological quantification of blood and lymph microvessels in prostate cancer. Its relevance for the anti-angiogenetic therapy. *Current Cancer Therapy Reviews*, 10(1), 1–12. https://doi.org/10.2174/1573394711001140815151624

Egevad, L., Mazzucchelli, R. & Montironi, R. (2012) Implications of the International Society of Urological Pathology modified Gleason grading system. *Archives of Pathology and Laboratory Medicine*, 136(4), 426–434. https://doi.org/10.5858/arpa.2011-0495-RA

Epstein, J.I., Allsbrook, W.C. Jr, Amin, M.B., Egevad, L.L. & Committee, I.G. (2005). The 2005 International Society of Urological Pathology (ISUP) Consensus Conference on Gleason Grading of Prostatic Carcinoma. *The American Journal of Surgical Pathology*, 29(9), 1228–1242. https://doi.org/10.1097/01.pas.0000173646.99337.b1

Eslahi, A., Noorafshan, A., Safarpour, A.R., Sepehrimanesh, M., Ariafara, A. & Nadimi, E. (2017) Stereological comparison of intraprostatic injection of alcohol and bleomycin with finasteride gavages in rats. *Central European Journal of Urology*, 70(2), 163–169. https://doi.org/10.5173/ceju.2017.1211

Fontana, F., Moretti, R.M., Raimondi, M., Marzagalli, M., Beretta, G., Procacci, P. et al. (2019) Delta-Tocotrienol induces apoptosis, involving endoplasmic reticulum stress and autophagy, and paraptosis in prostate cancer cells. *Cell Proliferation*, 52(3), e12576. https://doi.org/10.1111/cpr.12576.

Gómez, V., Ingelmo, I., Martín, R., Codesal, J., Rodríguez, R., Pozuelo, J.M. et al. (2009) Effect of prolactin on the population of epithelial cells from ventral prostate of intact and cyproterone acetate-treated peripubertal rats: stereological and immunohistochemical study. *Anatomical Record (Hoboken)*, 292(5), 746–755. https://doi.org/10.1002/ar.20879

Gundersen, H.J.G., Bagger, P., Bendtsen, T.F., Evans, S.M., Korbo, L., Marcussen, N. et al. (1988) The new stereological tools: disector, fractionator, nucleator and point sampled intercepts and their use in pathological research and diagnosis. *Acta Pathologica, Microbiologica, et Immunologica Scandinavica*, 96(10), 857–881. https://doi.org/10.1111/j.1699-0463.1988.tb00954.x

Howard, C.V. & Reed, M.G. (2005) *Unbiased stereology: three-dimensional measurement in microscopy*. Oxford: Bios Scientific Publishers, pp. 1–277.

Humphrey, P.A. (2004) Gleason grading and prognostic factors in carcinoma of the prostate. *Modern Pathology*, 17(3), 292–306. https://doi.org/10.1038/modpathol.3800054.

Iczkowski, K.A., Torkko, K.C., Kotnis, G.R., Wilson, R.S., Huang, W., Wheeler, T.M. et al. (2011) Pseudolumen size and perimeter in prostate cancer: correlation with patient outcome. *Prostate Cancer*, 2011, 1–5. https://doi.org/10.1155/2011/693853

Lambros, M.B., Seed, G., Sumanasuriya, S., Gil, V., Crespo, M., Fontes, M. et al. (2018) Single-cell analyses of prostate cancer liquid biopsies acquired by apheresis. *Clinical Cancer Research*, 24(22), 5635–5644. https://doi.org/10.1158/1078-0432.CCR-18-0862.

Leze, E., Maciel-Osorio, C.F. & Mandarim-de-Lacerda, C.A. (2014) Advantages of evaluating mean nuclear volume as an adjunct parameter in prostate cancer. *PLoS One*, 9(7), e102156. https://doi.org/10.1371/journal.pone.0102156.

Martin, J.J., Martin, R., Codesal, J., Fraile, B., Paniagua, R. & Santamaria, L. (2001) Cadmium chloride-induced dysplastic changes in the ventral rat prostate: an immunohistochemical and quantitative study. *Prostate*, 46(1), 11–20. https://doi.org/10.1002/1097-0045(20010 1)46:1<11:aid-pros1003>3.0.co;2-k

Mattfeldt, T., Gottfried, H.W., Wolter, H., Schmidt, V., Kestler, H.A. & Mayer, J. (2003) Classification of prostatic carcinoma with artificial neural networks using comparative genomic hybridization and quantitative stereological data. *Pathology, Research and Practice*, 199(12), 773–784. https://doi.org/10.1078/0344-0338-00496

Mattfeldt, T., Trijic, D., Gotffried, H.W. & Kestler, H.A. (2004) Incidental carcinoma of the prostate: clinicopathological, stereological and immunohistochemical findings studied with logistic regression and self-organizing feature maps. *British Journal of Urology International*, 93(3), 284–290. https://doi.org/10.1111/j.1464-410x.2004.04603.x

Mohammad, R.M., Muqbil, I., Lowe, L., Yedjou, C., Hsu, H.-Y., Lin, L.-T. et al. (2015) Broad targeting of resistance to apoptosis in cancer. *Seminars in Cancer Biology*, 35(Suppl), S78–S103. https://doi.org/10.1016/j.semcancer.2015.03.001.

Nagle, R.B., Ahmann, F.R., McDaniel, K.M., Paquin, M.L., Clark, V.A. & Celniker, A. (1987) Cytokeratin characterization of human prostatic carcinoma and its derived cell lines. *Cancer Research*, 47(1), 281–286.

Panahi, S., Abdollahifar, M.-A., Aliaghaei, A., Nazarian, H., Paktinat, S., Abdi, S. et al. (2017) Application of stereological methods for unbiased estimation of sperm morphology in the mice induced by busulfan. *Anatomy and Cell Biology*, 50(4), 301–305. https://doi.org/10.5115/acb.2017.50.4.301.

Park, S., Ang, R.R., Duffy, S.P., Bazov, J., Chi, K.N., Black, P.C. et al. (2014) Morphological differences between circulating tumor cells from prostate cancer patients and cultured prostate cancer cells. *PLoS One*, 9(1), e85264. https://doi.org/10.1371/journal.pone.0085264.

Real, M.V.F., Rocha, M.J., Goncalves, J.F. & Rocha, E. (2020) Histology and design-based estimation of hepatocellularity and volumes of hepatocytes in control and ethynylestradiol exposed males of platyfish (*Xiphophorus maculatus*). *Tissue and Cell*, 63, 101327. https://doi.org/10.1016/j.tice.2019.101327

Ribeiro, D.L., Marques, S.F.G., Alberti, S., Spadella, C.T., Manzato, A.J., Taboga, S.R. et al. (2008) Malignant lesions in the ventral prostate of alloxan-induced diabetic rats. *International Journal of Experimental Pathology*, 89(4), 276–283. https://doi.org/10.1111/j.1365-2613.2008.00591.x

Santamaria, L., Andres Delgado, L., Chaves, I., Ingelmo, I. & Teba, F. (2017) Stereological estimates of length and surface densities of the acini from normal and pathological prostate: global and local differences. *Histology and Histopathology*, 32(Suppl 1), 98.

Santamaria, L., Ingelmo, I., Ruiz, J. & Teba, F. (2011) Study of the distribution of microvessels in normal and pathologic prostate using an information-based similarity analysis. *Journal of Microscopy*, 243(3), 303–314. https://doi.org/10.1111/j.1365-2818.2011.03508.x

Santamaria, L., Ingelmo, I., Ruiz, J., Teba, F., Herranz, L.M., Montalban, G. et al. (2009) Stereological estimate of the length of microvessels and the number, proliferation and apoptosis of endothelial cells in prostate cancer. *The Open Prostate Cancer Journal*, 2, 46–53. https://doi.org/10.2174/1876822900902010046.

Santamaria, L., Ingelmo, I., Sinues, B., Martinez, L. & Teba, F. (2018) Quantification of the heterogeneity of cytokeratin 18 immunoexpression in prostate adenocarcinoma and normal prostate: global and local features. *Histology and Histopathology*, 33(10), 1099–1110. https://doi.org/10.14670/HH-18-009

Santamaria, L., Ingelmo, I., Teba, F., Coloma, A. & Martínez, L. (2016) Quantitative stereological estimations of structural patterns of the glandular tree in benign hyperplasia of prostate. *Open Journal of Pathology*, 6, 122–133 https://doi.org/10.4236/ojpathology.2016.63015

Santamaria Solis, L., Ingelmo Ingelmo, I., Rodriguez Ramos, R., Sinues Ojas, B., Martinez Blazquez, L. & Teba del Pino, F. (2015) Estimate of the K function and isotropy of acini in human normal prostate and prostate adenocarcinoma. *Histology and Histopathology*, 30(Suppl 1), 149–150.

Schlegel, R., Banks-Schlegel, S. & Pinkus, G.S. (1980) Immunohistochemical localization of keratin in normal human tissues. *Laboratory Investigation*, 42(1), 91–96.

Sorensen, F.B. (1991) Stereological estimation of the mean and variance of nuclear volume from vertical sections. *Journal of Microscopy*, 162(Pt 2), 203–229. https://doi.org/10.1111/j.1365-2818.1991.tb03132.x

Sterio, D.C. (1984) The unbiased estimation of number and sizes of arbitrary particles using the disector. *Journal of Microscopy*, 134(Pt 2), 127–136. https://doi.org/10.1111/j.1365-2818.1984.tb02501.x

Tolkach, Y. & Kristiansen, G. (2018) The heterogeneity of prostate cancer: a practical approach. *Pathobiology*, 85(1–2), 108–116. https://doi.org/10.1159/000477852.

Tschanz, S.A., Burri, P.H. & Weibel, E.R. (2011) A simple tool for stereological assessment of digital images: the STEPanizer. *Journal of Microscopy*, 243(1), 47–59. https://doi.org/10.1111/j.1365-2818.2010.03481.x

van Royen, M.E., Verhoef, E.I., Kweldam, C.F., van Cappellen, W.A., Kremers, G.-J., Houtsmuller, A.B. et al. (2016) Three-dimensional microscopic analysis of clinical prostate specimens. *Histopathology*, 69(6), 985–992. https://doi.org/10.1111/his.13022.

Verhoef, E.I., van Cappellen, W.A., Slotman, J.A., Kremers, G.-J., Ewing-Graham, P.C., Houtsmuller, A.B. et al. (2019) Three-dimensional analysis reveals two major architectural subgroups of prostate cancer growth patterns. *Modern Pathology*, 32(7), 1032–1041. https://doi.org/10.1038/s41379-019-0221-0.

Vilamaior, P.S., Taboga, S.R. & Carvalho, H.F. (2006) Postnatal growth of the ventral prostate in Wistar rats: a stereological and morphometrical study. *The Anatomical Record Part A: Discoveries in Molecular, Cellular, and Evolutionary Biology*, 288A(8), 885–892. https://doi.org/10.1002/ar.a.20363.

Wang, Z.P., Eisenberger, M.A., Carducci, M.A., Partin, A.W., Scher, H.I. & Ts'o, P.O. (2000) Identification and characterization of circulating prostate carcinoma cells. *Cancer*, 88(12), 2787–2795. https://doi.org/10.1002/1097-0142(20000615)88:12<2787:aid-cncr18>3.0.co;2-2.

West, M.J. (2012) *Basic stereology for biologists and neuroscientists*. New York: Cold Spring Harbor Laboratory Press, pp. 1–203.

Winter, R.N., Kramer, A., Borkowski, A. & Kyprianou, N. (2001) Loss of caspase-1 and caspase-3 protein expression in human prostate cancer. *Cancer Research*, 61(3), 1227–1232.